Cell

Consequences of Motor Copy Number on the Intracellular Transport of Kinesin-1-Driven Lipid Droplets

George T. Shubeita,[1,4,6] Susan L. Tran,[2,3,5,6] Jing Xu,[1] Michael Vershinin,[1] Silvia Cermelli,[1] Sean L. Cotton,[3] Michael A. Welte,[2,3,5,7,*] and Steven P. Gross[1,7,*]

[1]Department of Developmental and Cell Biology, University of California Irvine, Irvine, CA 92697, USA
[2]Department of Biology, University of Rochester, Rochester, NY 14627, USA
[3]Department of Biology and Rosenstiel Medical Research Center, Brandeis University, Waltham, MA 02454, USA
[4]Present address: Center for Nonlinear Dynamics and Department of Physics, University of Texas at Austin, Austin, TX 78712, USA
[5]Present address: Department of Biology, University of Rochester, Rochester, NY 14627, USA
[6]These authors contributed equally to this work
[7]These authors contributed equally to this work
*Correspondence: michael.welte@rochester.edu (M.A.W.), sgross@uci.edu (S.P.G.)
DOI 10.1016/j.cell.2008.10.021

SUMMARY

The microtubule motor kinesin-1 plays central roles in intracellular transport. It has been widely assumed that many cellular cargos are moved by multiple kinesins and that cargos with more motors move faster and for longer distances; concrete evidence, however, is sparse. Here we rigorously test these notions using lipid droplets in *Drosophila* embryos. We first employ antibody inhibition, genetics, biochemistry, and particle tracking to demonstrate that kinesin-1 mediates plus-end droplet motion. We then measure how variation in kinesin-1 expression affects the forces driving individual droplets and estimate the number of kinesins actively engaged per droplet. Unlike in vitro, increased motor number results in neither longer travel distances nor higher velocities. Our data suggest that cargos in vivo can simultaneously engage multiple kinesins and that transport properties are largely unaffected by variation in motor number. Apparently, higher-order regulatory mechanisms rather than motor number per se dominate cargo transport in vivo.

INTRODUCTION

Intracellular transport along microtubules is powered by molecular motors of the kinesin and cytoplasmic dynein families. Most kinesins travel toward the plus ends of microtubules, whereas dynein travels toward minus ends. Frequently, kinesins and dyneins are attached to the same cargo, but engage with the microtubule alternatively, resulting in constant back-and-forth cargo motion. Such bidirectional transport is widespread and has been observed for mitochondria, melanosomes, various vesicles, neurofilaments, ribonucleoprotein granules, and viruses (reviewed in Welte, 2004). Because distinct bidirectional cargos exhibit very similar motion characteristics, the regulatory mechanisms to control such transport might be quite general (reviewed in Gross, 2004).

Cells modulate net directionality and speed of bidirectional transport in response to extrinsic and intrinsic cues. Because net transport is determined by whether—on average—plus-end or minus-end travel distances are longer, the key to understanding transport regulation is to determine how cargo travel distances are controlled. Although molecules important for travel length control are being identified, it remains unclear how they affect the activities of their ultimate targets, the motors.

Studies in vitro suggest one possible mechanism: these regulators might modulate the number of motors active per cargo. In vitro, single molecules of kinesin-1 or dynein can travel ~1 μm along microtubules, either on their own or when attached to glass or plastic beads. Beads moved by multiple copies of such motors travel much further (Mallik et al., 2005; Vershinin et al., 2007).

Although important in vitro, the relevance of motor copy number for transport in vivo remains unclear, in large part because measuring the number of motors active per cargo is challenging. It is not sufficient to determine bulk levels of motors cofractionating with particular cargos, because motor number might vary from cargo to cargo or even on a single cargo over time. Furthermore, not every motor physically present on a cargo contributes to motion, either because it might not contact the track or because its activity is regulated. The crucial parameter to determine is the number of *engaged* motors.

Because motors in vitro slow down if opposed by a significant load, some studies infer motor number from the velocity that cargos display in vivo: faster cargos are assumed to have more motors engaged (Hill et al., 2004; Kural et al., 2005; Levi et al., 2006). However, the relationship between velocity and motor number is likely complex: the loads that cargos experience in vivo might not be high enough to explain observed velocity variations, and it is unresolved whether velocities are also modulated by regulatory factors (see Supplemental Data available online). It therefore remains unclear to what extent variation in the number of engaged motors controls either velocity or travel distances in vivo. It is not

even conclusively established that a cellular cargo can indeed employ more than one motor at a time.

In this article, we estimate the number of engaged motors using a direct measure, the force needed to stall a moving cargo. Theoretical considerations predict that such stall forces are proportional to the number of engaged motors (Kunwar et al., 2008), a notion confirmed in vitro for both kinesin-1 (Vershinin et al., 2007) and cytoplasmic dynein (Mallik et al., 2005). To implement this strategy in vivo, we analyzed lipid droplets in *Drosophila* embryos. Lipid droplets move bidirectionally along microtubules, and stall forces for individual droplets can be determined using optical tweezers (G.T.S. et al., unpublished data).

Plus-end droplet transport is developmentally regulated: during embryogenesis, plus-end travel distances vary, whereas minus-end travel lengths remain fixed (Gross et al., 2000; Welte et al., 1998). Thus, the plus-end motor appears to be the best candidate to explore a possible link between regulation of travel distance and motor copy number. However, only the minus-end droplet motor, cytoplasmic dynein (Gross et al., 2000), has been identified, whereas the plus-end motor is unknown.

Here we employ multiple independent approaches to show that droplet plus-end motion is powered by kinesin-1. We then manipulate kinesin-1 expression and determine how droplet stall forces are affected. These studies allow us to show, for the first time, that cargos in vivo can engage more than one copy of kinesin. We further find that an increase in motor number does not lead to an increase in droplet travel distance and that developmental regulation of transport is not accomplished by changes in motor copy number.

RESULTS

Kinesin-1 Is Required for Net Droplet Transport

In the early *Drosophila* embryo, lipid droplets move along radially arranged microtubules, which are oriented with the plus ends toward the center of the embryo and the minus ends toward the periphery. Because lipid droplets are large organelles that scatter light, transport-induced changes in droplet distribution dramatically alter the transparency of the embryo (Figure 1A and Movie S1). The peripheral cytoplasm is initially full of droplets and appears brown and hazy (phase I); although droplets are moving constantly, there is no net transport. In response to developmental signals (phase II, cycle 14 of embryogenesis), droplets undergo net inward (plus-end) transport, causing the periphery to turn transparent (a process called ''clearing''). An hour later (phase III), net outward (minus-end) droplet transport results in darkening of the periphery (''clouding''). Mutations that specifically disrupt transport of droplets demonstrate that clearing and clouding are indeed due to altered droplet distribution (Gross et al., 2003; Welte et al., 1998).

Circumstantial evidence suggested that the motor responsible for plus-end droplet motion might be kinesin-1. The plus-end droplet motor is maternally provided to embryos (Gross et al., 2003) and works in concert with cytoplasmic dynein (Gross et al., 2000). Similarly, kinesin-1 is maternally provided to the embryo (Brendza et al., 2000) and, in *Drosophila*, cooperates with cytoplasmic dynein in many cellular processes (e.g., Ling et al., 2004; Mische et al., 2007; Pilling et al., 2006).

Kinesin-1 is a heterotetramer, composed of two copies each of the kinesin heavy chain (Khc) and the kinesin light chain (Klc). To test whether kinesin-1 is required for droplet motion, we generated embryos that lack Khc. Because animals without any Khc die, we employed germ-line clone (GLC) technology with the protein null allele Khc^{27} to remove kinesin-1 function selectively during oogenesis (Serbus et al., 2005). Embryos laid by GLC mothers lack Khc (Figure 1B). Many of these embryos were morphologically abnormal, but a fraction (5%–10%) developed to phase II and exhibited a very opaque periphery, a phenotype indicating that lipid droplets failed to undergo inward (net plus-end) transport (Figure 1C). When Khc^{27} GLCs were generated in the presence of a transgene ($P\{Khc^{+}\}$) that provides wild-type Khc (Figure 1B), embryo development was rescued and inward droplet transport in phase II was restored (Figure 1C). Thus, aberrant droplet distribution in the Khc^{27} GLCs is due to lack of kinesin-1.

To detect lipid droplets specifically, we stained for the droplet-associated Klarsicht protein (Klar) (Guo et al., 2005). Klar accumulated basally in wild-type embryos, but was present throughout the periphery in Khc^{27} GLC embryos (Figure 1D). To validate that Klar marks droplets even when kinesin-1 is missing, we centrifuged embryos to separate lipid droplets from other organelles by density; the droplet-layer that forms at one side of the embryo is highly enriched in droplet proteins, including Klar (Guo et al., 2005). Klar is still droplet-associated in Khc^{27} GLC embryos (Figure 1E). Thus, both Klar staining and embryo opacity indicate that Khc^{27} GLC embryos do not support net plus-end droplet transport.

We also generated germ-line clones for a null allele of the other kinesin-1 subunit, Klc. Embryos that reached phase II failed to display net plus-end accumulation of lipid droplets, as determined by embryo opacity (Figure 1C) and Klar distribution (Figure 1D). Unlike certain light-chain independent cargos (Glater et al., 2006; Ling et al., 2004; Palacios and St Johnston, 2002), droplets apparently require both Khc and Klc for proper transport, similar to many membrane-bound vesicles.

Kinesin-1 Is Required for the Motion of Individual Droplets

Failure of net plus-end transport can be due to subtle changes in the relative run lengths of plus- and minus-end motion (Gross et al., 2003). We therefore analyzed the motion of individual droplets in the Khc^{27} GLC embryos. Droplet transport was dramatically reduced (Figure 2E): most droplets appeared to be stationary and only occasionally was there evidence for directed, yet still extremely limited, motion.

To quantify this impairment, we used a measure of average distance a droplet travels as a function of time, the mean square displacement (MSD) (Snider et al., 2004). For a droplet moving directionally, distance traveled is proportional to time, and so the MSD increases quadratically with time. For a diffusing particle, the MSD increases linearly. For droplet motion in wild-type embryos, the MSD was approximately quadratic; in the GLC embryos, it was greatly reduced and roughly linear, reminiscent of diffusion (Figure 2F). Because the MSD is insensitive to the *direction* of motion, droplets in the GLC embryos display

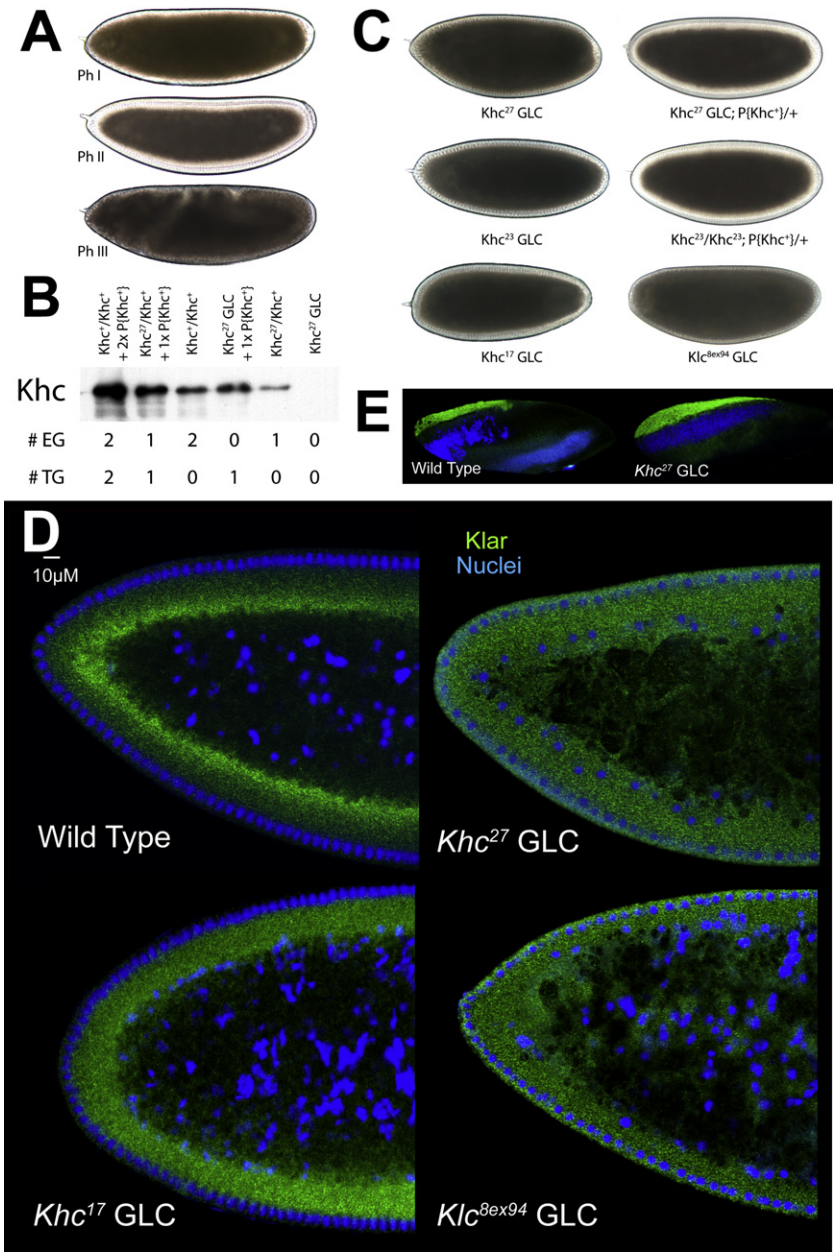

Figure 1. Net Transport of Lipid Droplets Requires Kinesin-1

(A) Lipid-droplet distribution in wild-type embryos, as revealed by transparency of the embryo periphery in transmitted light. During phases I (top) and III (bottom), the periphery is opaque because lipid droplets are present throughout. In phase II (middle), droplets move inward, and as a result the periphery is transparent ("clearing").

(B) Khc levels in embryos of various genotypes. Top: full description of genotypes; bottom: summary how many copies of the endogenous *Khc* gene (#EG) and the *Khc* transgene *P{Khc$^+$}* (#TG) are present. Proteins were extracted from embryos laid by mothers of the indicated genotypes, and Khc was detected by western analysis. Coomassie blue staining of membranes demonstrated equal protein loading across lanes (not shown).

(C) Kinesin-1 function is required for clearing of the embryonic periphery in phase II. Embryos that either completely lack one of the kinesin-1 subunits (*Khc^{27}* GLC and *Klc^{8ex94}* GLC) or contain only mutant kinesin (*Khc^{23}* GLC and *Khc^{17}* GLC) fail to undergo clearing during phase II. Expression of wild-type Khc (from the *P{Khc$^+$}* transgene) restores clearing in the absence of endogenous Khc (*Khc^{27}* GLCs) or when all endogenous Khc is mutant (embryos from mothers homozygous for *Khc^{23}*, rescued to viability by *P{Khc$^+$}*).

(D) Kinesin-1 function is required for net inward transport of lipid droplets in phase II. Embryos of various genotypes were stained for DNA (blue) and the droplet-marker Klar (green). In the wild-type, Klar accumulates basally, away from the peripheral nuclei (blue) in phase II, due to net plus-end droplet transport. When kinesin-1 is impaired (*Khc^{17}* GLC), Klar is uniformly distributed in the peripheral cytoplasm below the nuclei. When either of the kinesin-1 subunits is entirely absent (*Khc^{27}* or *Klc^{8ex94}* GLC), Klar is present not only throughout the peripheral cytoplasm, but also apical to nuclei and deep within the central yolk (where microtubules are not present). This severe mislocalization suggests that droplets are no longer attached to microtubules and diffuse throughout the embryo.

(E) Droplet association of Klar does not require kinesin-1. When embryos are centrifuged, the low-density lipid droplets accumulate in a distinct top layer, just above the nuclei (blue). Klar (green) is highly enriched in the droplet layer of both wild-type and *Khc^{27}* GLC embryos.

only minimal active motion in both the plus- and the minus-end direction.

Lack of motion might indicate absence of tracks. Immunostaining indicates that microtubules in *Khc^{27}* GLC embryos are less organized and extend farther internally in some embryonic regions, but overall microtubules are abundant, intact, and still radially arranged (Figure 2A). Embryos have some morphological defects (not shown), but microtubule integrity is sufficient to support cargo transport because yolk vesicles in *Khc^{27}* GLC embryos accumulate in the center (Figure S1); this process requires microtubules (Foe et al., 1993). We conclude that lack of droplet motion is not due to lack of microtubule tracks. Similarly, lack of tracks does not explain aberrant droplet transport in *Klc* GLC embryos because embryos that reached phase II had abundant microtubules (Figure 2A) and supported inward accumulation of yolk vesicles (not shown).

Partial Impairment of Kinesin-1 Function Is Sufficient to Alter Droplet Transport

The lack of droplet motion in the absence of kinesin-1 might indicate that during oogenesis kinesin-1 helps assemble the droplet transport machinery, consisting of some unknown plus-end motor and cytoplasmic dynein. Alternatively, kinesin-1 might directly power droplet motion, but—as observed in other instances of bidirectional transport—the activities of plus- and minus-end motors might be highly interdependent, so that impairment of one motor disrupts motion in both directions (Ling et al., 2004; Mische et al., 2007; Pilling et al., 2006). We found

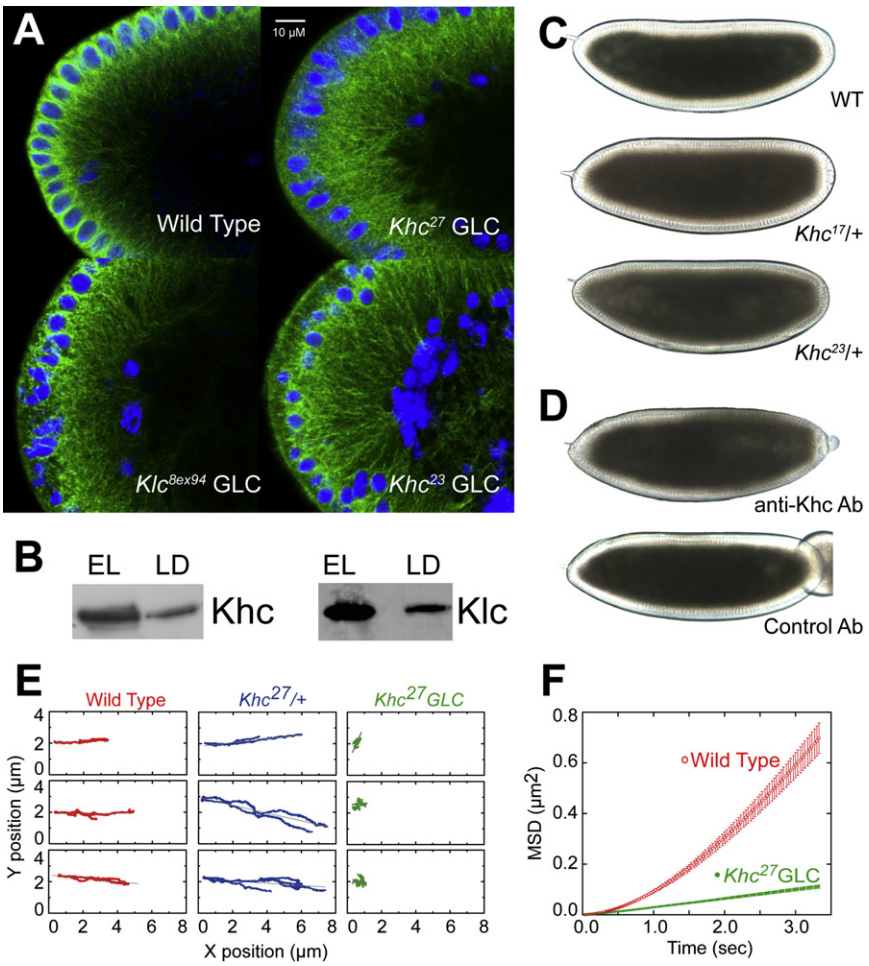

Figure 2. Kinesin-1 Is Directly Responsible for Droplet Motion

(A) Microtubule tracks are present in embryos with disrupted kinesin-1 function. Microtubules and nuclei were visualized by staining for β tubulin (green) and DNA (blue). Radially arranged microtubules are present in the embryo periphery of all genotypes shown, though their detailed arrangement is altered in the mutants: microtubules display less apical bundling (around the nuclei) and reach deeper into the embryos; sometimes regional patches are devoid of microtubules, possibly because nuclei failed to migrate to those regions earlier in development (not shown).

(B) Both subunits of kinesin-1 (Khc and Klc) are present on purified lipid droplets. Equal amounts of protein from total embryo lysate (EL) and biochemically purified lipid droplets (LD) were analyzed by western blotting. Droplets were purified as described previously (Cermelli et al., 2006).

(C) *Khc* alleles dominantly slow net droplet motion. Embryos from Khc^{17} or Khc^{23} heterozygous mothers (i.e., carrying both a mutant and a wild-type *Khc* allele) often display less efficient peripheral clearing in phase II than embryos from wild-type (top) mothers. Embryos shown are at very similar developmental stages (see Movie S1 for a time-lapse comparison). This clearing defect was variable in penetrance and severity; we estimate that at least half of embryos from either genotype were distinguishable from the wild-type.

(D) Acute inhibition of kinesin-1 promotes net minus-end droplet transport. Wild-type mid-phase II embryos were injected (on the right) with antibodies at concentrations of ~2–3 μg/μl. Embryos injected with a function-blocking antibody against Khc (top) rapidly turned opaque near the injection site, indicating outward motion of lipid droplets. Injection of a control antibody (bottom) had no effect.

(E) In the absence of Khc, droplet motion is severely impaired. Lipid droplets were tracked in phase II embryos; three sample traces are shown per genotype. Wild-type (WT) and Khc^{27}/+ embryos show similar traces with bidirectional transport; Khc^{27} GLCs display almost no directed motion.

(F) Droplets in Khc^{27} GLC embryos exhibit minimal directed motion, as assessed by the MSD as a function of time. The quadratic shape for wild-type (WT) indicates directed transport; the reduced, linear MSD for the Khc^{27} GLC embryos is reminiscent of diffusion. Error bars are standard errors of the mean.

that kinesin-1 is expressed during early embryogenesis when droplet transport occurs (Figures 1B and S2) and that it is present on biochemically purified lipid droplets (Figure 2B), supporting a direct role in droplet transport.

To disentangle direct kinesin-1 roles from roles in assembly of the transport machinery, we examined droplet motion when kinesin-1 is present but impaired. Khc^{23} and Khc^{17} encode full-length mutant kinesins that display reduced velocity of microtubule gliding in vitro (Brendza et al., 1999) and drive slower ooplasmic streaming in vivo (Serbus et al., 2005). GLC embryos for these alleles expressed abundant Khc (Figure S2E), had fewer morphological defects, and generally supported embryonic development better than the null allele (see also Serbus et al., 2005). In these embryos, microtubules were present (Figure 2A) and able to support inward transport of yolk vesicles (Figure S1) as well as membrane growth during cellularization (not shown).

In Khc^{17} GLC embryos, kinesin-1 is largely functional as the vast majority of such embryos develops into viable adults (Serbus et al., 2005) and lipid droplets displayed vigorous bidirectional motion (not shown). However, net plus-end droplet transport fails, because phase II embryos remain opaque (Figure 1C), and Klar is present throughout the periphery (Figure 1D). In addition, both travel distances (data not shown) and travel velocities (Figure S5) of plus-end motion were significantly reduced. These defects were much milder than when Khc is entirely lacking, both at the level of individual droplets (slower motion versus no motion) and of net transport (droplets were confined to the region between nuclei and yolk rather than displaced throughout the embryo; Figure 1D).

We observed an intermediate effect on droplet motion in Khc^{23} GLC embryos: droplets moved bidirectionally, but travel velocities were lower than for Khc^{17} (Figure S5). This is consistent with past reports (Serbus et al., 2005) that Khc^{23} impairs kinesin-1 activity more than Khc^{17}. These allele-specific effects on droplet motion are consistent with kinesin-1 directly moving the droplets. If kinesin-1 were simply delivering another motor to droplets, there would be no reason to expect allele-specific effects on velocity of transport.

Supporting evidence for a direct role of kinesin-1 comes from analysis of embryos that express both wild-type and mutant Khc (*Khc*^{17}/+ and *Khc*^{23}/+). In a subset of such embryos, clearing was less efficient than in the wild-type (Figure 2C and Movie S1), suggesting that the slower mutant kinesins dominantly interfere with droplet transport. We noticed no such impaired clearing in *Khc*^{27}/+ embryos (Movie S1) that express wild-type Khc at reduced levels (Figure 1B).

Acute Inhibition of Kinesin-1 Induces Net Minus-End Transport

If kinesin-1 powers droplet motion, acute kinesin-1 inhibition should alter transport. We employed a function-blocking antibody that recognizes Khc but not other kinesins (see Supplemental Data, antibody injections). This antibody was injected into wild-type embryos in mid-phase II, which had a functional transport machinery because droplets had already undergone net plus-end transport. Within 2 min or less after injection, the embryonic periphery in the vicinity of the injection site turned opaque, indicating net outward transport of droplets (Figure 2D, top). To achieve such a global redistribution requires significant net movement of the droplets within these 2 min, indicating that the actual change in droplet motion occurs much more rapidly, likely in seconds. Yolk vesicles remained in the interior. This effect was seen in essentially every injected embryo (n = 50–60 embryos in each of two experimental trials) and was specific: injection of a generic rabbit anti-chicken antibody failed to induce such transparency changes (Figure 2D, bottom). The rapidity of the net outward transport strongly suggests that kinesin-1 acts directly on lipid droplets and represents a core component of the transport machinery. Injection of the antibody apparently directly targets kinesin-1 and does not displace the rest of the motor machinery such as cytoplasmic dynein because the injected embryos display net minus-end droplet transport.

In summary, we conclude that kinesin-1 directly powers plus-end motion of lipid droplets. Although our data do not exclude that other plus-end motors might contribute to droplet transport, kinesin-1 clearly plays a dominant role because there is no plus-end droplet motion in *Khc* null embryos, specific acute inhibition of Khc is sufficient to induce net minus-end transport, and impaired Khc significantly reduces travel velocities.

Are Droplets Moved by One or Multiple Copies of Kinesin-1?

In vitro, the number of kinesins active per glass bead profoundly affects transport, including distances traveled and velocities under load (Vershinin et al., 2007). To understand kinesin-1-driven transport in vivo, it is thus crucial to know the number of active kinesins per cargo. The hypothesis that cargos in vivo employ multiple copies of the same motor (Gross et al., 2007) has been challenging to test directly (see Introduction).

In vitro motor stall forces are additive (Mallik et al., 2005; Vershinin et al., 2007), so measuring the forces generated by cargos could provide a read-out of how many motors are actively engaged. Stalls are measured at zero cargo velocity, so viscous/cytosolic drag does not affect such measurements. We previously employed optical tweezers to estimate droplet stall forces (Gross et al., 2000; Welte et al., 1998) and found that they vary in a quantized manner during embryogenesis. We therefore hypothesized that droplets are transported by multiple motors and that motor copy number changes developmentally. Although suggestive, other explanations could not be excluded; for example, the force generated by a single motor might be upregulated or downregulated in a stepwise manner.

The identification of kinesin-1 as the plus-end droplet motor allowed us to test the multiple-motor hypothesis. We determined whether reducing the overall amount of kinesin-1 alters droplet stall forces. If droplets normally carry a single kinesin-1 molecule, such a reduction should yield two droplet populations—some droplets that fail to move, and some that move with stall forces identical to the wild-type. But, if droplets are normally moved by multiple kinesins, this decrease should result in droplets driven by fewer kinesins and thus exhibiting reduced stall forces.

Droplets Can Engage Multiple Copies of Kinesin-1

We first developed an improved method to measure stall forces in vivo. Previously, we determined what fraction of lipid droplets escape from an optical trap at a set laser power (Welte et al., 1998). By varying laser power (and thus applied force), we extrapolated a mean stall force required to stop motion. This population measure cannot determine the force required to stall a particular cargo or correct for variations in cargo size. Here we precisely measure the force needed to stall *individual* lipid droplets (G.T.S. et al., unpublished data; see also Supplemental Data, force measurements). Typical stalls of a plus-end or minus-end moving droplet are shown in Figures 3A and 3B.

This new method reveals, for the first time, the *distribution* of stall forces for droplets. In vitro, multiple motors have a stall-force distribution with multiple peaks (Mallik et al., 2005; Vershinin et al., 2007). For plus-end moving droplets in vivo (Figure 3C), we observe two peaks, one at ~2.6 pN and one at ~5.2 pN. Although this distribution can be legitimately modeled as a bimodal distribution ($\chi^2 = 1.15952$, degrees of freedom [df] = 3; $p < 0.25$), it is not well described by a unimodal distribution ($\chi^2 = 22.86$, df = 6; $p > 0.999$). Because in vitro stall forces for kinesin-1 are approximately additive (Vershinin et al., 2007), we propose that these two peaks reflect the activity of one and two motors, respectively.

For minus-end moving droplets (Figure 3D), a peak at ~2.4 pN presumably represents the activity of a single motor. There is no well-resolved peak at 4.8 pN, but the increased weight in the histogram at forces larger than 4 pN (Figure 3D, arrows) is suggestive of the action of two motors. Investigating the details of minus-end stall forces is beyond the scope of this paper; however, the similarity in average stall force for minus- and plus-end moving droplets (4.0 ± 0.5 pN versus 3.9 ± 0.2 pN; Figures 4B and 4C) further suggests that future studies with more extensive statistics might reveal a second peak also for minus-end travel.

Force measurements on the same droplet over time provide independent evidence that changes in overall force production can be attributed to quick changes in the number of actively engaged motors. In Figure 3A, for example, a plus-end moving droplet stalls at 2.7 pN when the trap is switched on. After a few stalls and detachments (when the droplet falls back to

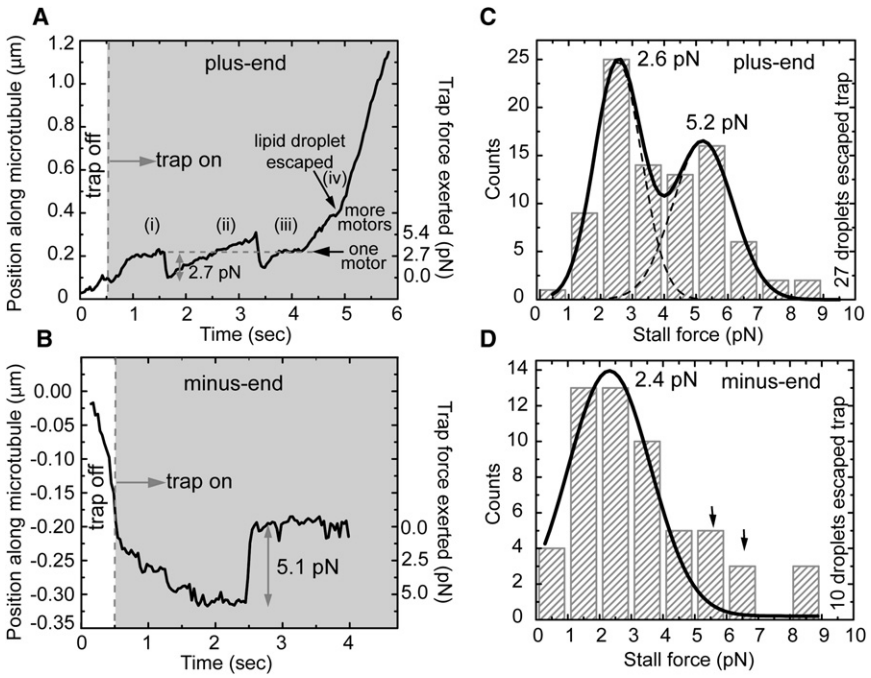

Figure 3. Quantifying Droplet Stall Forces

(A) Example of stalling a plus-end moving droplet. The droplet initially stalled at 2.7 pN, the motor detached, and it was pulled to the center of the trap (i). The droplet was subsequently driven out of the trap with more force, did not stall and prematurely fell back to the trap center (ii). After another stall at 2.7 pN (iii), more motors engaged and generated enough force to pull it out of the influence of the trap (iv).

(B) Example of stalling a minus-end moving droplet.

(C) Stall-force distribution for plus-end moving droplets in the wild-type. The histogram is fit (solid lines) with two Gaussian distributions centered at 2.6 and 5.2 pN. These values suggest that the peaks arise from lipid droplets moved by one and two motors, respectively. The fit did not include any restrictions on peak positions. Note that a number of droplets escape from the trap (rightmost bin), indicating the simultaneous action of even more motors.

(D) Stall-force distribution for minus-end moving droplets in the wild-type. The solid line is a Gaussian fit to the bins up to 4 pN. The bins above 4 pN (arrows) suggests a possible second peak (see text).

the center of the trap), the droplet escapes (this reflects a force exceeding the maximal trap force, i.e., > ~8 pN), suggesting that it is now pulled by additional motors.

We next decreased overall embryonic kinesin-1. In embryos from mothers heterozygous for the null allele *Khc*^{27}, bulk Khc levels were decreased ~50% relative to the wild-type (Figures

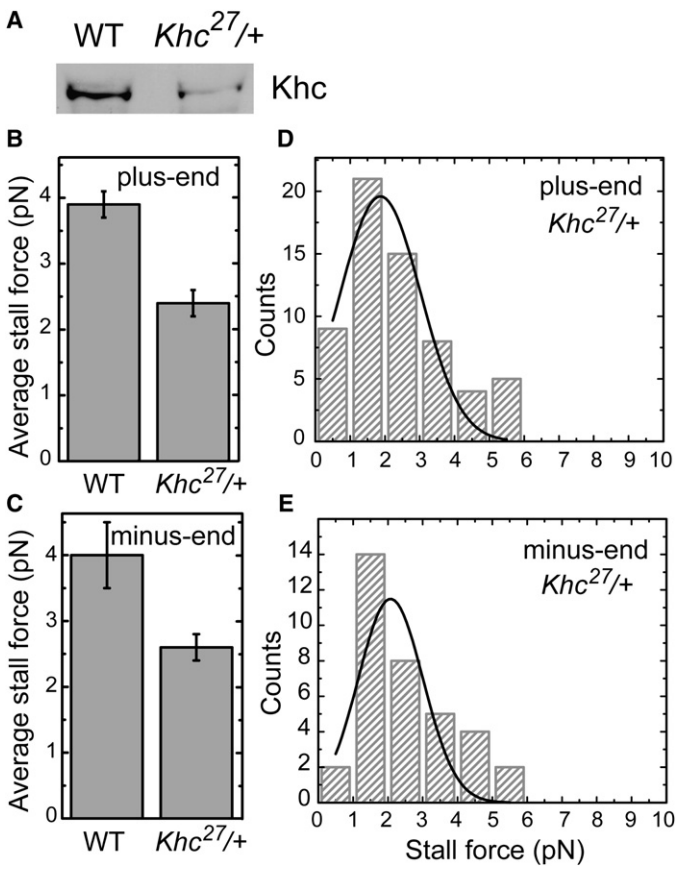

Figure 4. Droplets from *Khc*^{27}/+ Embryos Have Reduced Kinesin-1 Levels and Display Lower Stall Forces

(A) Khc levels on embryonic lipid droplets are reduced in Khc heterozygotes (*Khc*^{27}/+) compared with the wild-type (WT). Equal amounts of total protein from purified lipid droplets were analyzed for Khc by western blotting. This trend was reproduced in independent preparations; in some of them equal loading was additionally verified by probing for LSD2 (data not shown).

(B and C) Average stall forces in *Khc*^{27}/+ heterozygotes are reduced compared to the wild-type, both for plus-end (B) and minus-end (C) moving droplets.

(D and E) Stall-force distribution in *Khc*^{27}/+ heterozygotes for plus-end (D) and minus-end (E) moving droplets. Both histograms show a single prominent peak whose position coincides with the 2.6 ± 0.5 pN peak in Figure 3C, within the uncertainty estimated as half the bin size (plus-end: 1.9 ± 0.5 pN; minus-end 2.1 ± 0.5 pN). A diminished peak at 5.2 pN is expected given the reduced number of motors on the lipid droplets in heterozygous embryos compared with wild-type.

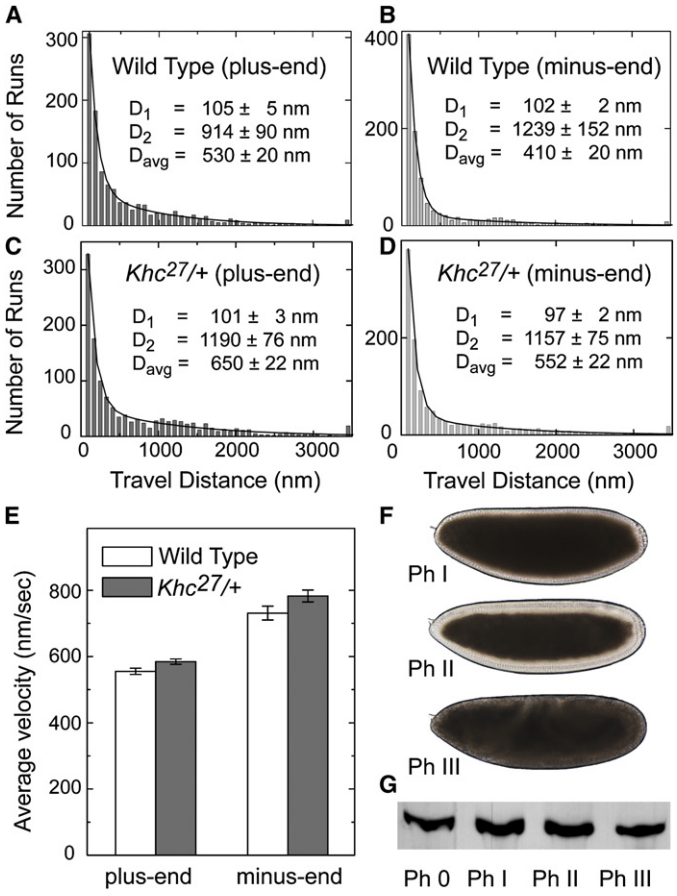

Figure 5. Droplet Motion in Wild-Type and *Khc*^{27}/+ Embryos Is Very Similar

(A–D) Distribution of lipid droplet run-lengths in wild-type (A, B) and *Khc*^{27}/+ (C, D) embryos. Using established approaches (see Experimental Procedures), we employed these distributions to quantify parameters of the two travel states droplets exhibit (Gross et al., 2000): D_1 = average travel distance of the short-slow state; D_2 = average travel distance of the long-fast state; D_{avg} = mean run length. For both directions of motion, the heterozygotes showed a slight but statistically significant *increase* in the mean run length ($p = 4.8 \times 10^{-3}$ for plus-end run lengths; $p = 7.27 \times 10^{-7}$ for minus-end run lengths; we used a two-sided rank-sum test because of data skewness).

(E) Mean travel velocities of lipid droplets for plus-end and minus-end motion. For both directions of motion, *Khc*^{27}/+ shows a slight but statistically significant *increase* in the mean velocity of long-fast travel ($p = 6.85 \times 10^{-3}$ for plus-end velocities; $p = 3.48 \times 10^{-2}$ for minus-end velocities; one-sided t test). Only runs longer than 500 nm in length were used to calculate average velocities. Error bars are standard errors of the mean.

(F) *Khc*^{27}/+ embryos display normal directionality of net droplet transport. Despite reduced Khc protein levels, these embryos display clearing in phase II and clouding in phase III, similar to the wild-type (Figure 1A and Movie S1).

(G) Khc levels on droplets remain constant during embryogenesis. Lipid droplets were purified from wild-type embryos of the indicated phases and analyzed for Khc as in Figure 4A.

1B, S2A, and S2B). We detected a similar decrease in Khc levels on purified lipid droplets (Figure 4A). Thus, the amount of droplet-bound kinesin-1 seems to be determined by bulk availability of kinesin-1 in the cytosol.

In these embryos, no increase in unmoving droplets was observed (not shown), suggesting that wild-type droplets carry enough potentially active motors that a 50% reduction in motor number leaves almost none of them without active motors. The mean force required to stall these moving droplets was significantly decreased (Figure 4B), and the distribution of stall forces showed a single prominent peak (Figure 4D; statistically, these data are distinct from those in Figure 3C; p value of Kolmogorov-Smirnov test = 2e-6; i.e., confidence > 99.99). Although the upper peak at ~5 pN is dramatically decreased, there are still a bit too many counts in the 5+ pN bins to be well modeled as unimodal distribution, and larger statistics would likely reveal a percentage of escaping droplets smaller than for wild-type. We conclude that in the mutant embryos, the number of engaged kinesins per droplets is reduced and wild-type droplets are frequently moved by multiple kinesins. To our knowledge, this is the first direct demonstration of multiple motors working together on the same cargo in vivo.

Activities of Kinesin-1 and Dynein Are Tightly Coupled

Intriguingly, in *Khc*^{27}/+ embryos, stall forces for minus-end moving droplets were also reduced (Figure 4B). Apparently, the activities of plus- and minus-end motors on droplets is very tightly coupled, an interpretation supported by the fact that during wild-type embryogenesis maximal droplet stall forces for plus- and minus-end motion increase and decrease in parallel (Welte et al., 1998). Coupling may improve robustness of transport (see Supplemental Data).

The mechanism mediating coupling remains unknown, and its analysis is beyond the scope of this paper. Preliminary evidence points to the possibility that dyneins and kinesins are added to droplets in pairs because lipid droplets isolated from *Khc*^{27} heterozygotes displayed variably reduced levels of the dynein subunit Dic in repeated trials (Figure S2C). Coupling apparently does not monitor motor activity per se: acute inhibition of kinesin-1 induces net minus-end transport (Figure 2D), indicating that dynein remains active.

Regardless of the mechanism of coupling, the reduced stall forces for both directions of motion in *Khc*^{27} heterozygotes allow us to ask for both kinesin-1 and cytoplasmic dynein how the number of engaged motors affects motion parameters like travel distances and travel velocities.

Travel Distances Are Not Reduced as the Number of Engaged Motors Decreases

In vitro, the number of motors per cargo greatly affects transport: more motors move further. If motion is opposed by significant load (e.g., from viscous drag), multimotor cargos are expected to move with higher velocities (Klumpp and Lipowsky, 2005; Kunwar et al., 2008) than cargos driven by just one motor. Our comparison of stall forces in wild-type and *Khc*^{27}/+ embryos allows us to test the in vivo relevance of these studies.

We quantified motion of individual droplets with high-resolution particle tracking (Carter et al., 2005). We focused on periods of uninterrupted motion ("runs," see Experimental Procedures), and determined travel velocities (see below) and overall distance traveled (run length) (Figures 5A–5D). Compared with the

wild-type, droplets in Khc^{27}/+ embryos did not move shorter distances. In fact, they displayed slight—but statistically significant—*increases* in mean travel distances. Thus, at least in the case of lipid droplets, in vivo travel distances are not limited by motor number. Because travel in neither direction was reduced, this conclusion applies to both kinesin-1 and cytoplasmic dynein. Consistent with these rather minor changes in transport parameters at the level of individual droplets, net droplet transport was similar in wild-type and Khc^{27}/+ embryos; in particular, the mutant embryos underwent cytoplasmic clearing in phase II and clouding in phase III (Figure 5F, Movie S1).

Reduced Motor Copy Number Causes Slightly Increased Travel Velocities

Based on simple models, it has been assumed that in vivo more motors will move a cargo faster (see Discussion). Here, we test this idea. Lipid droplets display two classes of runs in each direction: short-slow runs and long-fast runs. Because the short runs may represent motors engaged in a tug-of-war (Gross et al., 2000) and do not contribute significantly to overall transport, we focused our analysis on the velocity of long runs (i.e., those at least 500 nm long). For both plus- and minus-end motion, mean velocity in the Khc^{27}/+ embryos was ~5.5% *higher* than in wild-type embryos (Figure 5E). Although a relatively small effect, this is well outside the uncertainty of our measurements (see Supplemental Data, section 7). Although it seems counterintuitive that an increase in motor number (from Khc^{27}/+ to wild-type embryos) would reduce travel velocity, an increase of such a magnitude is predicted from a new theoretical model describing how multiple motors function under viscous load (Kunwar et al., 2008; see also Supplemental Data, section 7).

Kinesin-1 Levels on Droplets Do Not Display Significant Developmental Variation

During embryogenesis, three phases of droplet transport can be distinguished: phase I (motion, but no net transport), phase II (net plus-end transport), and phase III (net minus-end transport). Control of net transport involves increasing or decreasing plus-end travel distances while minus-end motion is relatively unaffected (Gross et al., 2000; Welte et al., 1998). If control of run lengths were achieved by regulating the number of kinesin-1 copies on droplets, one would expect increases in kinesin-1 levels in phase II and reduction in phase III. However, when we biochemically purified lipid droplets from wild-type embryos of different stages, we detected no obvious change in the amount of droplet-bound Khc (Figure 5G). The overall embryonic pool of Khc was also constant during these phases (Figure S2B). Together with the observation that decreasing the number of engaged motors by ~50% does not impair transport, we conclude that control of net droplet transport is not achieved by regulating kinesin copy number.

DISCUSSION

Kinesin-1 Drives Plus-End Motion of Lipid Droplets

We find that kinesin-1 is absolutely required for net plus-end transport of droplets and directly drives droplet motion. In *Caenorhabditis elegans* intraflagellar transport, plus-end motion reflects cooperation of two distinct plus-end motors (Pan et al., 2006). Our current data cannot rule out that plus-end lipid droplet motion involves the contribution of an unidentified motor in addition to kinesin-1. However, if such a motor exists, its activity apparently depends entirely on kinesin-1 because in the absence of Khc there is no motion. Even when Khc is present, impairing its activity (via mutations or antibody inhibition) is sufficient to prevent net plus-end transport (Figures 1D and 2D). These observations suggest that kinesin-1 dominates plus-end motion of droplets and that other kinesins, on their own, at most make a restricted contribution to transport (see Supplemental Data, section 1).

This identification of kinesin-1 as driving plus-end droplet motion underscores the importance of droplet motion as a general model system, since in most cases of bidirectional transport the plus-end motor is either kinesin-1 or kinesin-2.

Lipid Droplets Are Moved by Multiple Motors

Although it was widely assumed that cargos in vivo can engage multiple copies of the same motor (Gross et al., 2007), conclusive proof was lacking. Our data provide by far the strongest evidence yet for this hypothesis. How many of the lipid droplets are moved by multiple motors? The events represented by the 2.6 pN peak in Figure 3C encompass ~40% of all stall force measurements in the figure. If this peak indeed represents the activity of one motor per droplet, most droplets (~60%) actively engage two motors or more. It is conceivable that the 2.6 pN peak is due to the simultaneous activity of several (n) motors, with the 5.2 pN peak due to 2n motors. In this case, the fraction of droplets engaging two or more motors will be considerably higher.

Travel Distance Is Not Controlled by Motor Number

Both modeling (Klumpp and Lipowsky, 2005; Kunwar et al., 2008) and measurements in vitro (Vershinin et al., 2007) suggest that unless something additional interferes, cargos with two or more motors will travel for very long distances before falling off the tracks. With more than 60% of the droplets in vivo engaging at least two motors, such long travels should be frequent; they are, however, not observed (Gross et al., 2000). Thus, our determination that in vivo droplets are typically moved by multiple motors but move relatively short distances suggests that some additional factor is present in vivo that is absent in vitro.

This in vivo/in vitro difference might be explained by high cytosolic viscosity, because the resulting load could decrease both travel distance and velocity (Klumpp and Lipowsky, 2005). Cytosolic load has been invoked to account for variations in travel velocities of other intracellular cargos (Hill et al., 2004; Kural et al., 2005; Levi et al., 2006). But if viscous drag was limiting travel in the wild-type, it would be even more potent in Khc^{27}/+ embryos: with fewer motors sharing the same cytosolic drag, the increased per-motor load would impede travel further. However, because neither run lengths nor velocities are decreased, cytosolic drag cannot significantly limit droplet transport.

Alternatively, travel distances in vivo might be inherently shorter. But in vivo run lengths of single Kinesins not attached to cargo are similar to those measured in in vitro studies (Cai et al., 2007). In addition, if single-motor run lengths were limiting in Khc^{27}/+ embryos, then the additional engaged motors in the

wild-type would allow longer travels, a prediction not borne out by our experiments.

Droplet travel distances, therefore, appear not to be limited by inherent motor properties, but by distinct, higher-level mechanisms. We previously proposed the existence of a "switch" that actively terminates runs and thus cuts short the long travels expected from multiple engaged motors (Gross et al., 2000). Our new data reveal that the switch mechanism is rather insensitive to motor number: over a 2-fold range of engaged motors, parameters of motion change minimally. Although we currently favor the hypothesis that the switch mechanism reflects the activity of a complex that regulates motor activity and coordinates motors, a recent theoretical model (Müller et al., 2008) suggests that under some circumstances, an unregulated competition between opposite motors could lead to the switching behavior we observe. Our identification of the plus-end droplet motor and its in vivo properties will provide the basis for future studies to distinguish between these models.

Forces Produced by Single Motors In Vivo

Our previous population stall-force measurements (Welte et al., 1998) suggested that the force required to stall a single droplet motor (for either direction) was ~1.1 pN. The new data presented here lead us to conclude that this force is actually ~2.6 pN (Figure 3C). We envision two possible explanations for this difference in estimates. One possibility is our improved ability to identify truly stalled droplets. As droplets move against the load applied by the optical trap, they can prematurely detach from the microtubule, even before the motors experience maximal load (e.g., Figure 3A, feature (ii), and Figure S3); this occurs quite frequently. Our old measurements scored droplets as "trapped" if they failed to escape from the trap and thus included premature detachments; because this criterion overestimates the fraction of stalled droplets, this approach underestimates the stall force. In our new measurements, we monitor the position of the droplet relative to the trap center and only count events in which the droplet indeed stalls out; that is, the droplet slows down gradually and remains at a fixed position away from the trap center for a period. Because this criterion excludes premature detachments, these events do not inappropriately depress the calculated stall force. A second possibility is that in wild-type phase II embryos the single-motor state is rare and the 2.6 pN peak in Figure 3C represents the activity of two or more motors. If so, a single-motor force peak might become apparent if Khc expression can be reduced even further than in the Khc^{27}/+ embryos or when different phases of transport are examined, because stall forces vary developmentally (Welte et al., 1998).

The stall force for single kinesin-1 molecules in vitro is between 4 to 8 pN; recombinant *Drosophila* kinesin-1, in particular, generates ~5 pN (Carter and Cross, 2005). Our measurements put the effective stall force of a single kinesin-1 in vivo at ~2.6 pN (or even less). We believe that this difference accurately reflects distinct properties of kinesin-1-mediated transport in vivo and in vitro because our own in vitro kinesin-1 stall force measurements are ~5 pN (Vershinin et al., 2007), and we have extensively checked our calibration procedures (see Supplemental Data, force measurement). We speculate that cofactors present in vivo, but not in vitro, modulate the motor's force output.

Regulation of Multiple Motors In Vivo

In vivo, the distances motors travel are highly regulated: for bidirectional transport, such regulation determines net direction of transport. However, the mechanisms controlling run length remain unknown. Our analysis of droplet motion indicates that whereas cargos in vivo can simultaneously engage multiple motors, travel lengths do not dramatically increase as more motors are engaged, contrary to unregulated in vitro systems. Thus, alternative mechanisms can dominate run termination in vivo. Whether regulation of motor copy number tunes transport of *any* cargo remains an open question.

The mechanisms that terminate runs are an area of active investigation. For lipid droplets, four proteins are implicated: the dynein cofactor dynactin (Gross et al., 2002) and the novel protein Klar (Welte et al., 1998) might coordinate dynein and kinesin-1 activity (i.e., turn one motor off when the opposing motor is active). The transacting signal Halo (Gross et al., 2003) and the droplet-associated "conductor" LSD2 (Welte et al., 2005) mediate how travel distances change during development. Molecular dissection of these regulators and identification of their binding partners should reveal the mechanisms of run length control. Because these molecules and their orthologs are important for many other transport processes, these findings will likely illuminate the regulation of microtubule motors in general.

EXPERIMENTAL PROCEDURES

Fly Strains, Antibody Injections, and Western Blot Analysis

The wild-type stock was Oregon R; *Khc* and *Klc* germ-line clones were generated as previously described (Serbus et al., 2005; Palacios and St Johnston, 2002; see also Supplemental Data). For embryo injections, anti-Khc antibody was processed as previously described (Serbus et al., 2005) and injected using standard procedures (e.g., Gross et al., 2003). Antibody specificity and details for western blot analysis are described in Supplemental Experimental Procedures.

Immunolocalization and Microscopy

Yolk vesicles, Klar, microtubules, and DNA were detected as previously described (Gross et al., 2003; Guo et al., 2005; Sisson et al., 2000), using yolk autofluorescence, Klar-M or β-tubulin immunostaining, and Hoechst 33258, respectively. Embryo centrifugation was performed as described previously (Guo et al., 2005). To compare clearing progress between embryos of different genotypes, image sequences from time-lapse movies were aligned such that the frames representing the midpoint of cellularization (when membranes reach the basal tip of the nuclei) were synchronized.

Lipid-Droplet Tracking and Track Analysis

Quantification of droplet motion was performed in phase II during the clearing process, where droplets are on average moving toward the embryo center, and was done as previously described (Gross et al., 2000; see Supplemental Experimental Procedures for details). Run-length distributions and velocities were calculated from at least 8 embryos per genotype (an average of 30 ± 5 droplets tracked per embryo). Run-length distributions were fit by two exponential decays as detailed previously (Gross et al., 2000). The two decay lengths (D_1 and D_2) characterize the short and long run lengths, respectively. Both decay lengths as well as the average run length (D_{avg}) are shown in Figures 5A–5D.

Force Measurements

Experimental details of the stall-force measurements on individual lipid droplets will be published elsewhere (G.T.S. et al., unpublished data). Briefly, an optical trap setup was built atop an inverted optical microscope. For fast and precise alignment of the trap with the position of the lipid droplet, a

computer-controlled piezoelectric stage-mounted mirror was used in conjunction with a fast single-particle tracking program capable of real-time tracking of particles at rates exceeding 30 frames/sec (Carter et al., 2005). At the click of the mouse on the CCD camera image of a moving lipid droplet, the program determines the droplet's position with an accuracy of a few nanometers, triggers the piezo-driven mirror to move to that position and opens the shutter to trap the droplet. A cargo was scored as stalled if it remained stationary out of the center of the trap for $\geq$ 0.35 sec. More details, including trap calibration, are provided in the Supplemental Data.

SUPPLEMENTAL DATA

Supplemental Data include Supplemental Experimental Procedures, five figures, and one movie and are available with this article online at http://www.cell.com/supplemental/S0092-8674(08)01313-5.

ACKNOWLEDGMENTS

We thank the Bloomington Stock Center, B. Saxton, and I. Palacios for fly stocks, B. Theurkauf and B. Cha for advice on antibody microinjections, N. Rizzo for help with western analysis, and A. Müller and D. Lambert for comments on the manuscript. This work was supported by NIGMS grant GM 64624 (to S.P.G.) and NIGMS grant GM64687 and start-up support from the University of Rochester (to M.A.W). G.T.S. was a Paul Sigler/Agouron Fellow of the Helen Hay Whitney Foundation.

Received: April 14, 2008
Revised: August 8, 2008
Accepted: October 6, 2008
Published: December 11, 2008

REFERENCES

Brendza, K.M., Rose, D.J., Gilbert, S.P., and Saxton, W.M. (1999). Lethal kinesin mutations reveal amino acids important for ATPase activation and structural coupling. J. Biol. Chem. *274*, 31506–31514.

Brendza, R.P., Serbus, L.R., Duffy, J.B., and Saxton, W.M. (2000). A function for kinesin I in the posterior transport of oskar mRNA and Staufen protein. Science *289*, 2120–2122.

Cai, D., Verhey, K.J., and Meyhofer, E. (2007). Tracking single kinesin molecules in the cytoplasm of mammalian cells. Biophys. J. *92*, 4137–4144.

Carter, B.C., Shubeita, G.T., and Gross, S.P. (2005). Tracking single particles: a user-friendly quantitative evaluation. Phys. Biol. *2*, 60–72.

Carter, N.J., and Cross, R.A. (2005). Mechanics of the kinesin step. Nature *435*, 308–312.

Cermelli, S., Guo, Y., Gross, S.P., and Welte, M.A. (2006). The lipid-droplet proteome reveals that droplets are a protein-storage depot. Curr. Biol. *16*, 1783–1795.

Foe, V.E., Odell, G.M., and Edgar, B.A. (1993). Mitosis and morphogenesis in the Drosophila embryo. In The Development of Drosophila melanogaster, M. Bate and A. Martinez-Arias, eds. (Cold Spring Harbor, NY: Cold Spring Harbor Laboratory Press), pp. 149–300.

Glater, E.E., Megeath, L.J., Stowers, R.S., and Schwarz, T.L. (2006). Axonal transport of mitochondria requires milton to recruit kinesin heavy chain and is light chain independent. J. Cell Biol. *173*, 545–557.

Gross, S.P. (2004). Hither and yon: a review of bi-directional microtubule-based transport. Phys. Biol. *1*, R1–R11.

Gross, S.P., Guo, Y., Martinez, J.E., and Welte, M.A. (2003). A determinant for directionality of organelle transport in Drosophila embryos. Curr. Biol. *13*, 1660–1668.

Gross, S.P., Vershinin, M., and Shubeita, G.T. (2007). Cargo transport: two motors are sometimes better than one. Curr. Biol. *17*, R478–R486.

Gross, S.P., Welte, M.A., Block, S.M., and Wieschaus, E.F. (2000). Dynein-mediated cargo transport in vivo: a switch controls travel distance. J. Cell Biol. *148*, 945–956.

Gross, S.P., Welte, M.A., Block, S.M., and Wieschaus, E.F. (2002). Coordination of opposite-polarity microtubule motors. J. Cell Biol. *156*, 715–724.

Guo, Y., Jangi, S., and Welte, M.A. (2005). Organelle-specific control of intracellular transport: distinctly targeted isoforms of the regulator Klar. Mol. Biol. Cell *16*, 1406–1416.

Hill, D.B., Plaza, M.J., Bonin, K., and Holzwarth, G. (2004). Fast vesicle transport in PC12 neurites: velocities and forces. Eur. Biophys. J. *33*, 623–632.

Klumpp, S., and Lipowsky, R. (2005). Cooperative cargo transport by several molecular motors. Proc. Natl. Acad. Sci. USA *102*, 17284–17289.

Kunwar, A., Vershinin, M., Xu, J., and Gross, S.P. (2008). Stepping, strain gating, and an unexpected force-velocity curve for multiple-motor based transport. Curr. Biol. *18*, 1173–1183.

Kural, C., Kim, H., Syed, S., Goshima, G., Gelfand, V.I., and Selvin, P.R. (2005). Kinesin and dynein move a peroxisome in vivo: a tug-of-war or coordinated movement? Science *308*, 1469–1472.

Levi, V., Serpinskaya, A.S., Gratton, E., and Gelfand, V. (2006). Organelle transport along microtubules in Xenopus melanophores: evidence for cooperation between multiple motors. Biophys. J. *90*, 318–327.

Ling, S.C., Fahrner, P.S., Greenough, W.T., and Gelfand, V.I. (2004). Transport of Drosophila fragile X mental retardation protein-containing ribonucleoprotein granules by kinesin-1 and cytoplasmic dynein. Proc. Natl. Acad. Sci. USA *101*, 17428–17433.

Mallik, R., Petrov, D., Lex, S.A., King, S.J., and Gross, S.P. (2005). Building complexity: an in vitro study of cytoplasmic dynein with in vivo implications. Curr. Biol. *15*, 2075–2085.

Mische, S., Li, M., Serr, M., and Hays, T.S. (2007). Direct observation of regulated ribonucleoprotein transport across the nurse cell/oocyte boundary. Mol. Biol. Cell *18*, 2254–2263.

Müller, M.J., Klumpp, S., and Lipowsky, R. (2008). Tug-of-war as a cooperative mechanism for bidirectional cargo transport by molecular motors. Proc. Natl. Acad. Sci. USA *105*, 4609–4614.

Palacios, I.M., and St Johnston, D. (2002). Kinesin light chain-independent function of the Kinesin heavy chain in cytoplasmic streaming and posterior localisation in the Drosophila oocyte. Development *129*, 5473–5485.

Pan, X., Ou, G., Civelekoglu-Scholey, G., Blacque, O.E., Endres, N.F., Tao, L., Mogilner, A., Leroux, M.R., Vale, R.D., and Scholey, J.M. (2006). Mechanism of transport of IFT particles in C. elegans cilia by the concerted action of kinesin-II and OSM-3 motors. J. Cell Biol. *174*, 1035–1045.

Pilling, A.D., Horiuchi, D., Lively, C.M., and Saxton, W.M. (2006). Kinesin-1 and dynein are the primary motors for fast transport of mitochondria in Drosophila motor axons. Mol. Biol. Cell *17*, 2057–2068.

Serbus, L.R., Cha, B.J., Theurkauf, W.E., and Saxton, W.M. (2005). Dynein and the actin cytoskeleton control kinesin-driven cytoplasmic streaming in Drosophila oocytes. Development *132*, 3743–3752.

Sisson, J.C., Field, C., Ventura, R., Royou, A., and Sullivan, W. (2000). Lava lamp, a novel peripheral golgi protein, is required for Drosophila melanogaster cellularization. J. Cell Biol. *151*, 905–918.

Snider, J., Lin, F., Zahedi, N., Rodionov, V., Yu, C.C., and Gross, S.P. (2004). Intracellular actin-based transport: how far you go depends on how often you switch. Proc. Natl. Acad. Sci. USA *101*, 13204–13209.

Vershinin, M., Carter, B.C., Razafsky, D.S., King, S.J., and Gross, S.P. (2007). Multiple-motor based transport and its regulation by Tau. Proc. Natl. Acad. Sci. USA *104*, 87–92.

Welte, M.A. (2004). Bidirectional transport along microtubules. Curr. Biol. *14*, R525–R537.

Welte, M.A., Cermelli, S., Griner, J., Viera, A., Guo, Y., Kim, D.H., Gindhart, J.G., and Gross, S.P. (2005). Regulation of lipid-droplet transport by the perilipin homolog LSD2. Curr. Biol. *15*, 1266–1275.

Welte, M.A., Gross, S.P., Postner, M., Block, S.M., and Wieschaus, E.F. (1998). Developmental regulation of vesicle transport in Drosophila embryos: forces and kinetics. Cell *92*, 547–557.